Treatments of Inhomogeneous Clouds in a GCM Column Radiation Model

L. Oreopoulos and R. F. Cahalan
Joint Center for Earth Systems Technology
University of Maryland
Baltimore, Maryland

M. Khairoutdinov
Department of Atmospheric Sciences
Colorado State University
Fort Collins, Colorado

L. Oreopoulos, M.-D. Chou, and R. F. Cahalan
Laboratory of Atmospheres
National Aeronautics and Space Administration
Goddard Space Flight Center
Greenbelt, Maryland

H. W. Barker
Meteorological Service of Canada
Downsview, Ontario

Introduction

The main purpose of this abstract is to evaluate the performance under inhomogeneous cloud conditions of the Column Radiation Models (CORAMs) developed by Chou and collaborators (see references), and used in various NASA-Goddard General Circulation Models (GCMs). Testing more sophisticated research versions of the CORAM that account for cloud inhomogeneity is secondary, and relevant findings will be shown only for the shortwave (SW) CORAM (we note however that algorithms that take into account the inhomogeneous nature of clouds at the infrared part of the spectrum have also been developed, see Li and Barker 2002). The CORAMs are evaluated on global scales, but with the caveat that the input cloud data come from only one of 500 simulated days. Still, this is an improvement over previous studies where assessments of the errors of this type of plane-parallel homogeneous (PPH) codes were made using a limited number of cloud fields generated either by theoretical models (e.g., Cahalan et al. 1994) or by Cloud Resolving Models (CRMs) attempting to simulate the clouds of a specific field campaign (e.g., Barker et al. 1999).

Dataset: CAM/CRM Clouds

Recently, Khairoutdinov et al. (2003) embedded a two-dimensional (2D) version of the three-dimensional (3D) CRM described in detail by Khairoutdinov and Randall (2003) into each grid column of a realistic GCM, the NCAR Community Atmosphere Model (CAM; the atmospheric component of the Community Climate System Model) version 1.8, to serve as a super-parameterization of clouds (for earlier implementations of this concept see Khairoutdinov and Randall 2001). We have selected a single day (January 1) from a 500-day long simulation with the super-parameterization, initialized on September 1st, using T42 resolution (2.8° x 2.8° grid) and 26 vertical layers (24 for the CRM itself, at the same levels as the lowest 24 layers of the CAM). The cloud fields that are used as input in our

radiative transfer calculations with the CORAMs come from 24 global "snapshots" saved at 1-hour intervals for this day. Within each of the 64 x 128 gridboxes covering the globe, clouds are then resolved in 64 columns, of 4 km horizontal width (aligned in the west-east direction) and 24 vertical layers.

Figure 1 shows latitude-height (zonally-averaged) cross sections of ensemble-mean (averaged over 24 snapshots) cloud properties at each model layer: cloud fraction, water path, and cloud inhomogeneity parameter ν of Barker (1996) calculated from the method of moments (MOM) as the square of the ratio of mean to standard deviation of the water path of each layer. These figures show that the super parameterization captures the main contrast in cloud types between tropics and mid-latitudes: clouds in the tropics are higher in the troposphere, thicker, and more heterogeneous (smaller values of ν).

The Column Radiation Models

We use both the SW and LW CORAMs developed by M.-D. Chou and collaborators and used in NASA-GSFC GCMs. The latest versions of the codes can be downloaded from the World Wide Web address http://climate.gsfc.nasa.gov/~chou. This website also provides the accompanying NASA technical documents that describe the CORAMs (Chou and Suarez 1999; Chou et al. 2001). For the SW CORAM the reader can also refer to Chou et al. (1998). Some of the most recent changes in the SW CORAM are the inclusion of variable cloud particle size that depends on water content, following McFarquhar (2001) for ice clouds and Szczodrak et al. (2001) for water clouds, and of a new parameter–ization for ice cloud single-scattering albedo (Chou et al. 2002). We will discuss the implications of the first of these changes in our calculations in the following section. Another important feature of the SW CORAM is the way cloud overlap is treated and which is schematically presented in Figure 2. Clouds are grouped in three categories: low, middle, and high, separated at 700 and 400 hPa. Through an optical depth adjustment that preserves the layer albedo for direct and diffuse incident radiation, the cloud in any layer that has smaller cloud fraction than the maximum cloud fraction within its group, is "stretched" and "thinned" until it acquires that maximum cloud fraction value (details can be found in Chou et al. 1998). After this adjustment, each cloud group has a unique cloud fraction associated with it, and the cloud groups are assumed to overlap randomly. This overlap assumption allows each gridbox to be divided into $\leq 2^n$ sub-columns ($n \leq 3$) where each layer is either completely cloudy or cloud-free, and for which the full vertical distribution of fluxes is calculated. The weighted average of the sub-column estimates gives the mean for the entire gridbox, and can be thought of as"crude" Independent Column Approximation (ICA).

For LW calculations the concept of the probability of clear line-of-sight of Harshvardhan et al. (1987) is used to calculate the flux transmittance between two different layers. Clouds are again grouped in three different height ranges, as in Figure 2, with maximum overlap assumed within each group, and random overlap between groups. Probabilities of clear line-of-sight are calculated for each group, and the total probability between any two levels is the product of probabilities of the groups contained within these levels. For details see Chou et al. (2001).

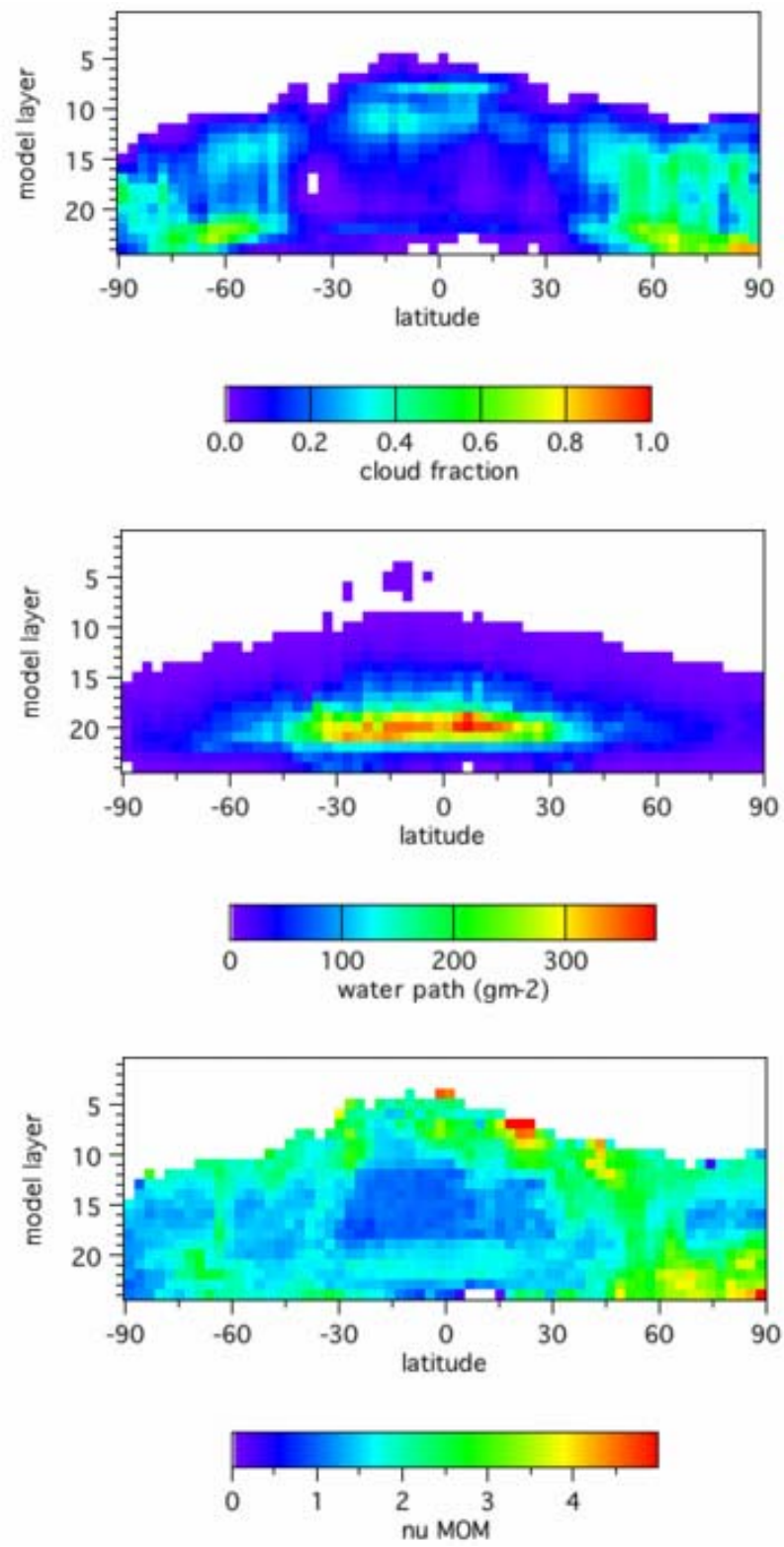

Figure 1. Ensemble- and zonally- averaged values of layer cloud fraction, water path, inhomogeneity parameter χ, and inhomogeneity parameter ν.

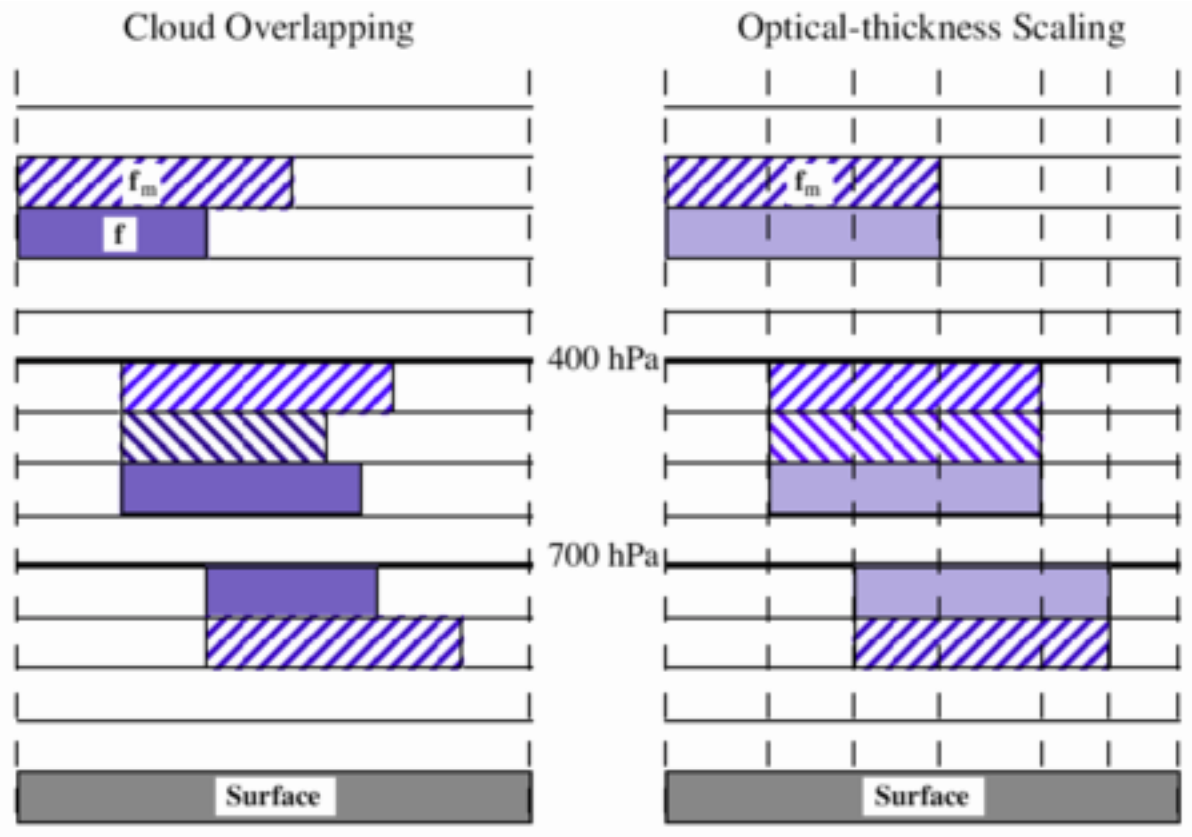

Figure 2. Sketch of how cloud overlap and optical thickness scaling is implemented in the SW CORAM (from Chou et al. 1998).

SW Experiments

For our broadband SW calculations we performed four different ensembles of runs: two ensembles with the original version of the CORAM and two with modified versions. The original version was used for ICA and PPH runs. The ICA runs were performed as follows: the CORAM was run for each sub-column in which each layer was either overcast or cloud-free and had a particle size profile that depended on the water content profile according to McFarquhar (2001) and Szcodrak et al. (2001), as explained above; the gridbox mean fluxes were derived by averaging the results for the 64 columns. Note that the discussion pertaining to Figure 2 is irrelevant due to the nature of the ICA. The PPH runs were performed as follows: for each vertical layer the cloud fraction and the mean liquid and ice water paths were determined for the gridbox; the particle sizes were estimated from the mean water paths; the CORAM run for each gridbox using as input these cloud fraction, water path, and particle size profiles.

One of the modified versions of the CORAM, called “PPH random” was designed to reveal the impact of the cloud adjustment and overlap assumption depicted in Figure 2. In this PPH variant, the upward and downward fluxes of each layer were calculated as the weighted average of the corresponding clear and cloudy fluxes. The flux profile was then determined by radiatively linking these average layer fluxes. As explained in Oreopoulos and Barker (1999), because this type of linking does not contain any

information on whether the transmitted or reflected flux to a layer comes from the clear or cloudy parts of the layers above or below, it is in practice equivalent to a random overlap assumption for all layers, regardless of whether they are contiguous or not.

The other modified version is based on the Gamma Weighted Two Stream Approximation (GWTSA) of Oreopoulos and Barker (1999) where the direct beam and δ-Eddington PPH solutions are replaced with their counterpart analytic solutions obtained by integrating over a gamma distribution of optical depths. The actual implementation in the Goddard SW CORAM is different than that described in Oreopoulos and Barker (1999): first, the scaling of optical of Figure 2 is retained; second, the cloud optical adjust–ment described in their paper by eq. (21-22) is omitted; third, MOM estimates of ν are used instead of maximum likelihood estimates; and fourth, ν is estimated from the water path variability. This value is not identical to the value derived from the optical depth variability, as was the case in Oreopoulos and Barker (1999) that used a constant particle size assumption. Estimating ν from the water path variability simplifies matters since the spectral dependence in optical depth does not translate to spectral dependence in ν, and is more consistent with possible future implementations of GWTSA in GCMs, which are not expected to predict subgrid particle size variability.

Our runs used a realistic global distribution of solar zenith angles (SZAs) for each snapshot correspond–ing to January 1. Thus, we can express the results of the performance of the CORAM in energy units Wm^{-2}. The SW surface albedo was approximated as being spectrally independent and unaffected by SZA variations or the presence of clouds (which largely regulate the relative amounts of direct to diffuse solar irradiance reaching the ground). The broadband values from a February 1-5 simulation of the Meteo France ARPEGE GCM were used (Räisänen 1999), interpolated from T42 resolution to the 2.8° resolution of the super parameterization experiments (Räisänen 2003, personal communication).

Figure 3 shows the globally averaged mean errors relative to the ICA for the three different versions of the SW CORAM and for the following quantities: reflected flux at TOA (RTOA), net flux absorbed at the surface (NSFC), and net flux absorbed by the atmosphere (ATMA). Averages are shown for all gridboxes as well as overcast gridboxes (~1500) only ("ovc"). Figure 4 shows the zonally averaged mean and root mean square (rms) errors for RTOA, and Figure 5 shows the zonally averaged heating rate errors. Results are ensemble-averaged over all 24 snapshots, and negative mean error values indicate overestimate relative to the ICA.

LW Experiments

The LW CORAM was only used unmodified with ICA and PPH runs performed using the methodology described above for the SW experiments. Note that in the ICA calculations the subgrid variability of temperatures had a negligible influence on the results and was ignored. The broadband surface emissiveties of Räisänen (1999) were used with surface temperatures set equal to the average temperature of the lowest CRM layer. Figure 6 shows the globally averaged mean and rms errors of PPH for all gridboxes and for overcast gridboxes only, for the following quantities: outgoing LW radiation (OLR), net flux absorbed at the surface (NSFC), and net flux absorbed by the atmosphere (ATMA). Figure 7 shows zonally-averaged results for the same quantities, and Figure 8 shows zonally-

averaged cooling rate PPH errors. Results are ensemble-averaged over all 24 snapshots, and negative mean error values indicate overestimate relative to the ICA.

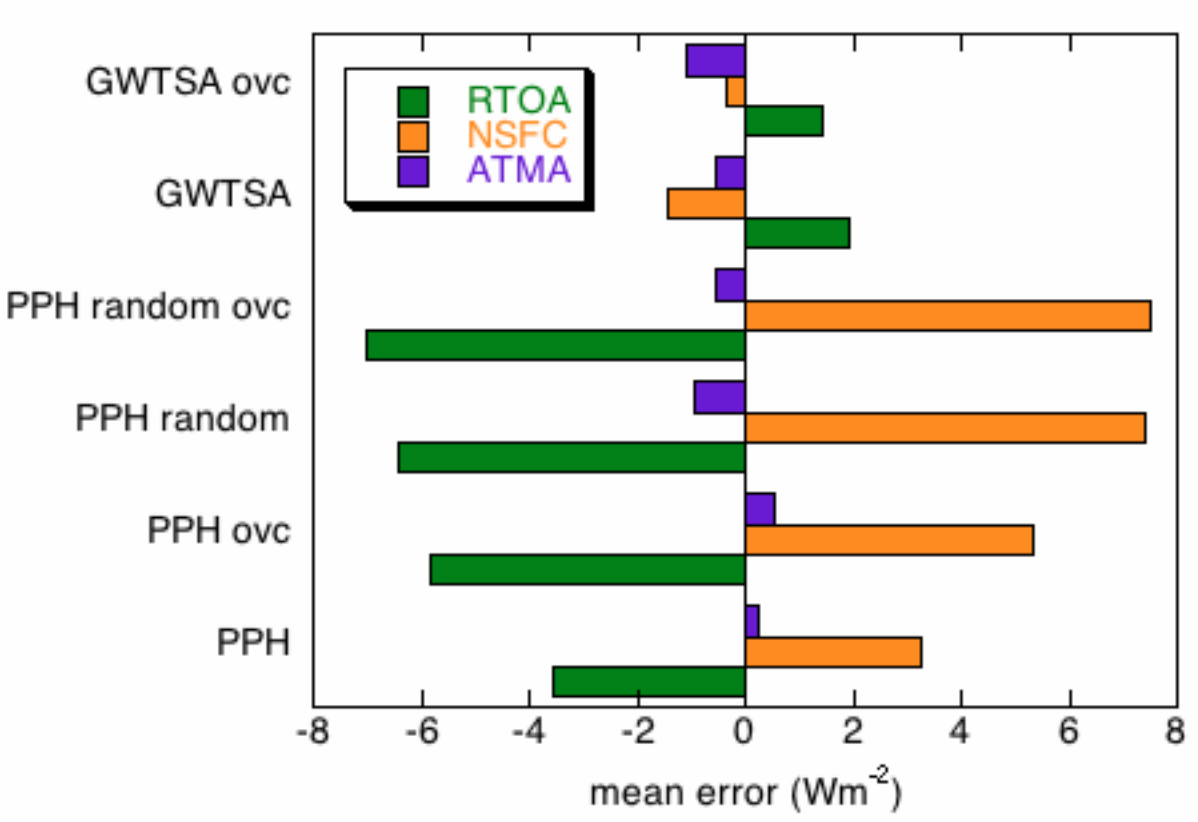

Figure 3. Globally-averaged SW flux errors. "ovc" is for overcast gridboxes only.

Discussion and Conclusions

The results shown in this abstract illustrate the generally good performance of the SW and LW CORAMs currently implemented in a variety of GSFC GCMs. In the SW case, even with no subgrid variability information provided for the PPH calculation, the global mean errors do not exceed 4 Wm^{-2} for fluxes at the atmospheric boundaries and 0.3 Wm^{-2} for the flux absorbed within the atmosphere.

Zonal heating rate errors are always below 0.3 K/d with overestimates for high clouds and under–estimates for low clouds. Errors are larger in the tropics where the thickest and most inhomogeneous clouds can be found, and larger in the S. H. than in the N. H., mainly because of the greater available solar energy. PPH overestimates reflected flux and underestimates by almost the same amount the flux absorbed at the surface, the net result being very small errors in the flux absorbed by the atmosphere. When the scaling of optical depth and the overlap assumptions associated with it are removed, the deterioration in performance is notable. On the other hand, implementation of the GWTSA results in significant improvements.

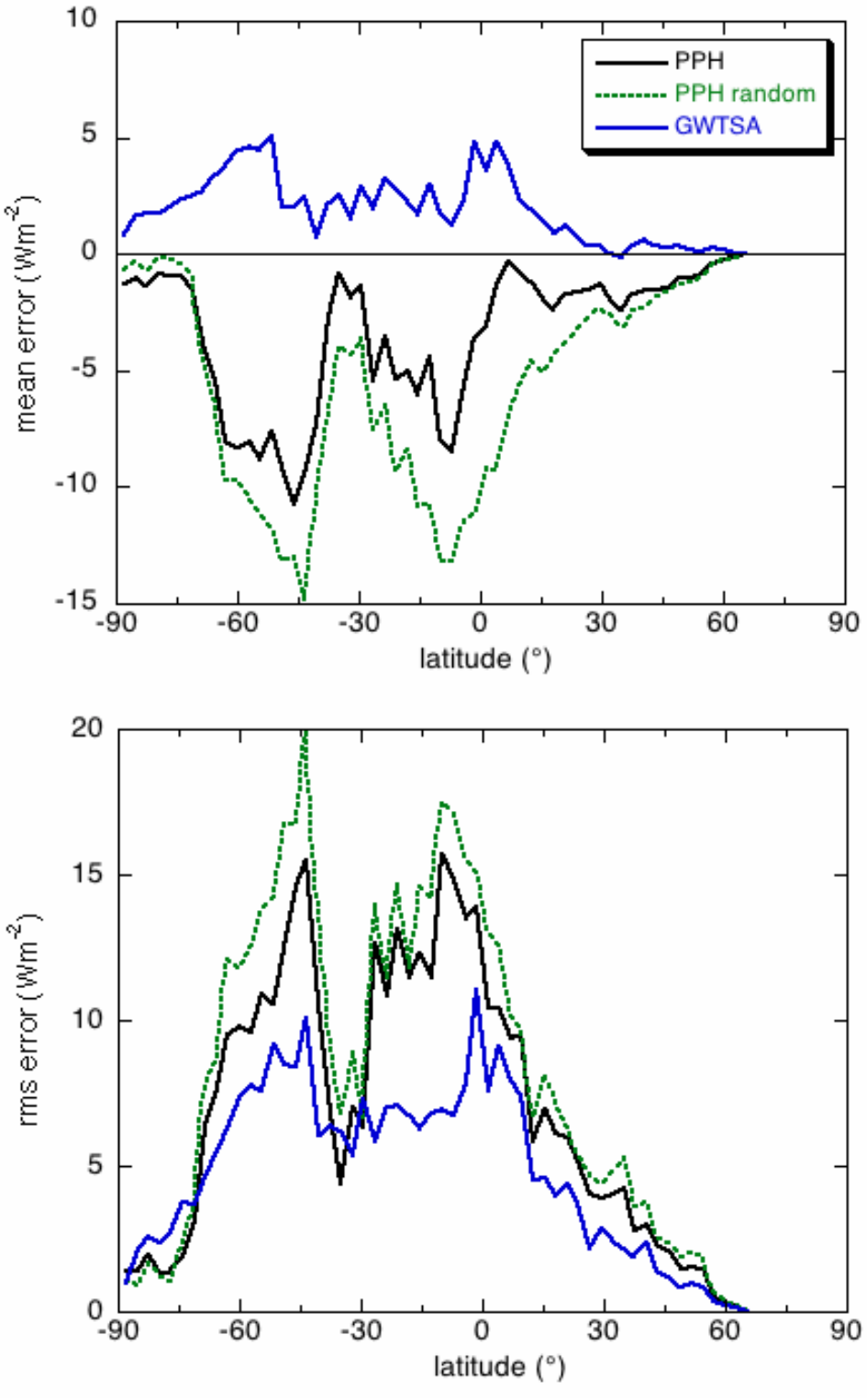

Figure 4. Zonally-averaged SW flux errors for RTOA.

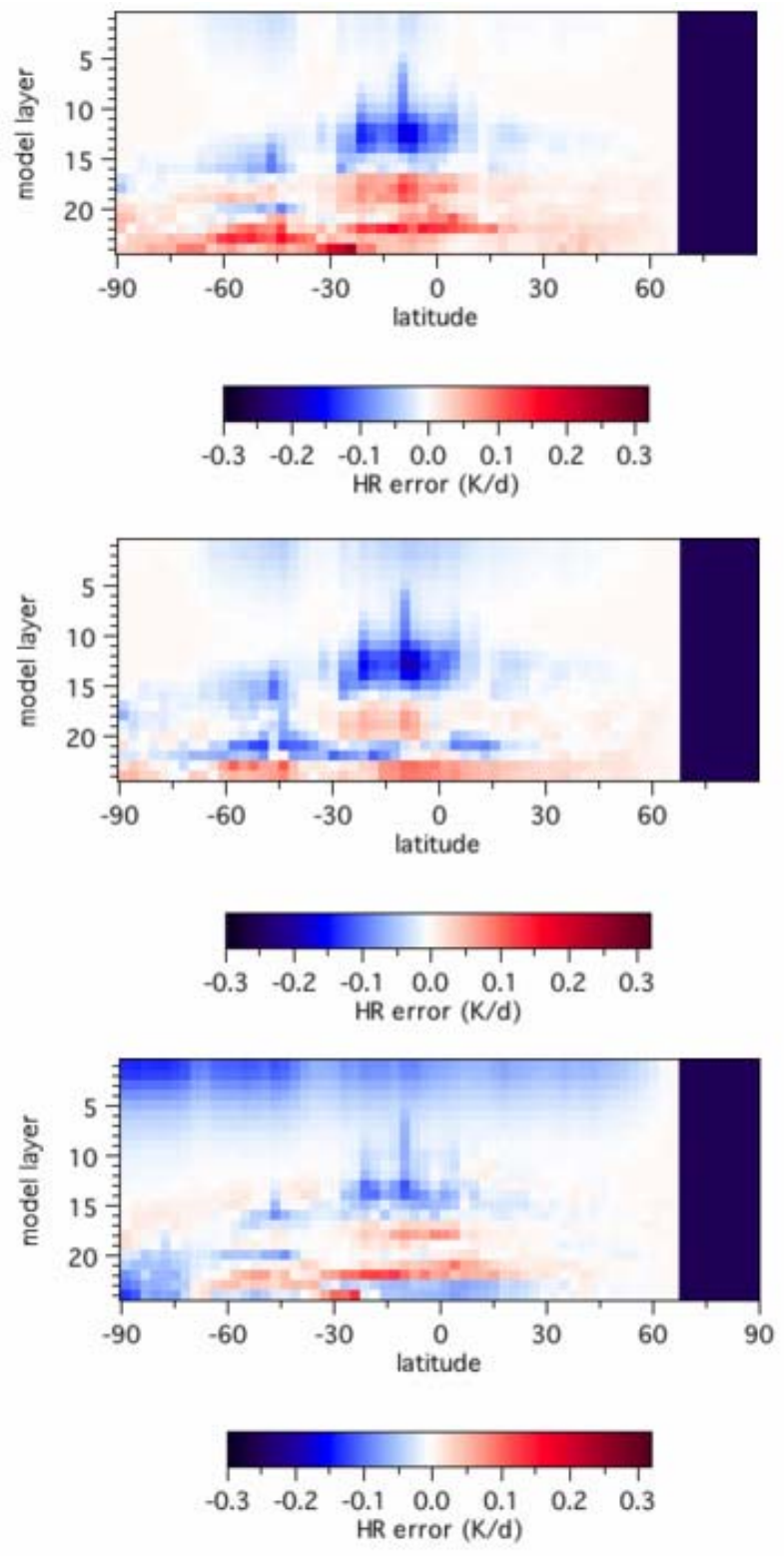

Figure 5. Zonally-averaged SW heating rate errors. Top: PPH; Middle: PPH random; Bottom: GWTSA. There are no values available above ~68°N because there is no illumination.

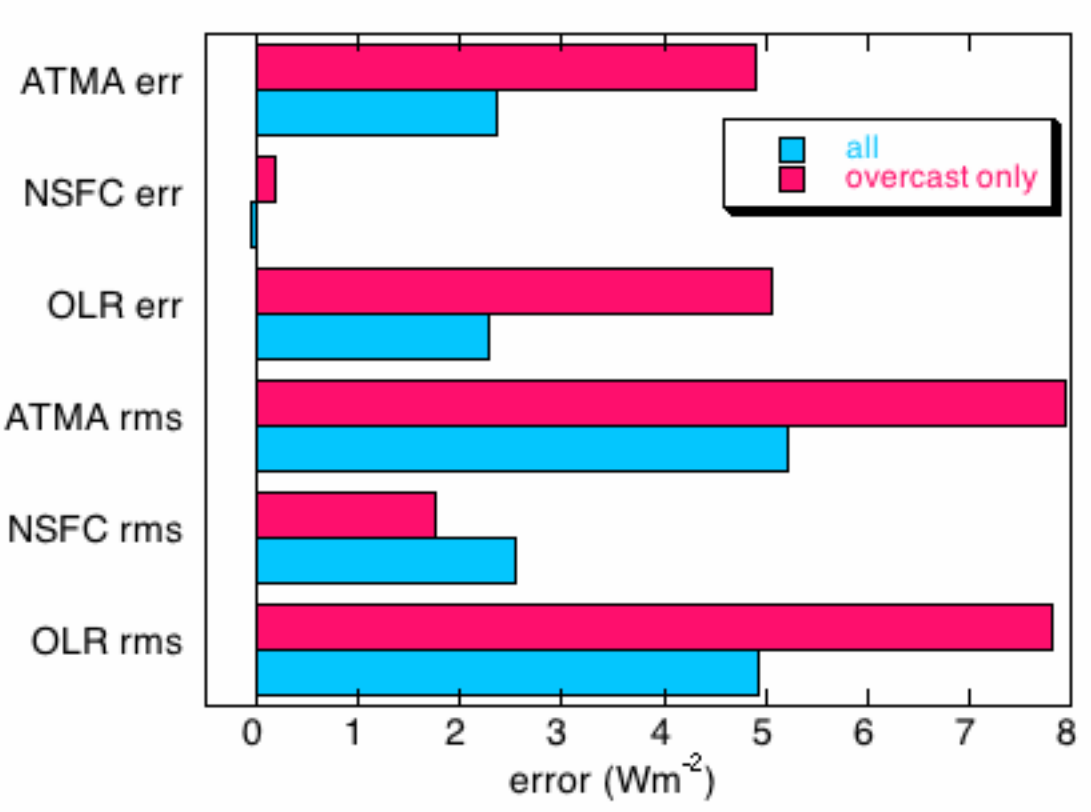

Figure 6. Globally-averaged LW flux errors of PPH.

In the LW case, PPH overestimates OLR and absorbed flux in the atmosphere by equal amounts (~2 Wm^{-2} at global scales), and is almost perfect for the net flux at the surface (although this is the net result of overestimates at low and underestimates at high latitudes). Again, the largest flux errors occur in the tropics where cloud heterogeneity is more pronounced. The cooling rates tend to be over–estimated by the PPH at the higher and underestimated at the lower tropospheric levels, but errors are always below 0.6 K/d.

These results suggest that previous studies demonstrating the inaccuracy of plane-parallel models may have unfairly focused on worst scenario cases, and that current radiative transfer algorithms of GCMs may be more capable than previously thought in estimating realistic spatial and temporal averages of radiative fluxes (as long as they are provided with correct cloud profiles). However, even if the errors of the particular model are small, they seem to be systematic, and the impact of the introduced bias can only be assessed with climate simulations.

Corresponding Author

Lazaros Oreopoulos, lazaros@climate.gsfc.nasa.gov, (301)614-6128

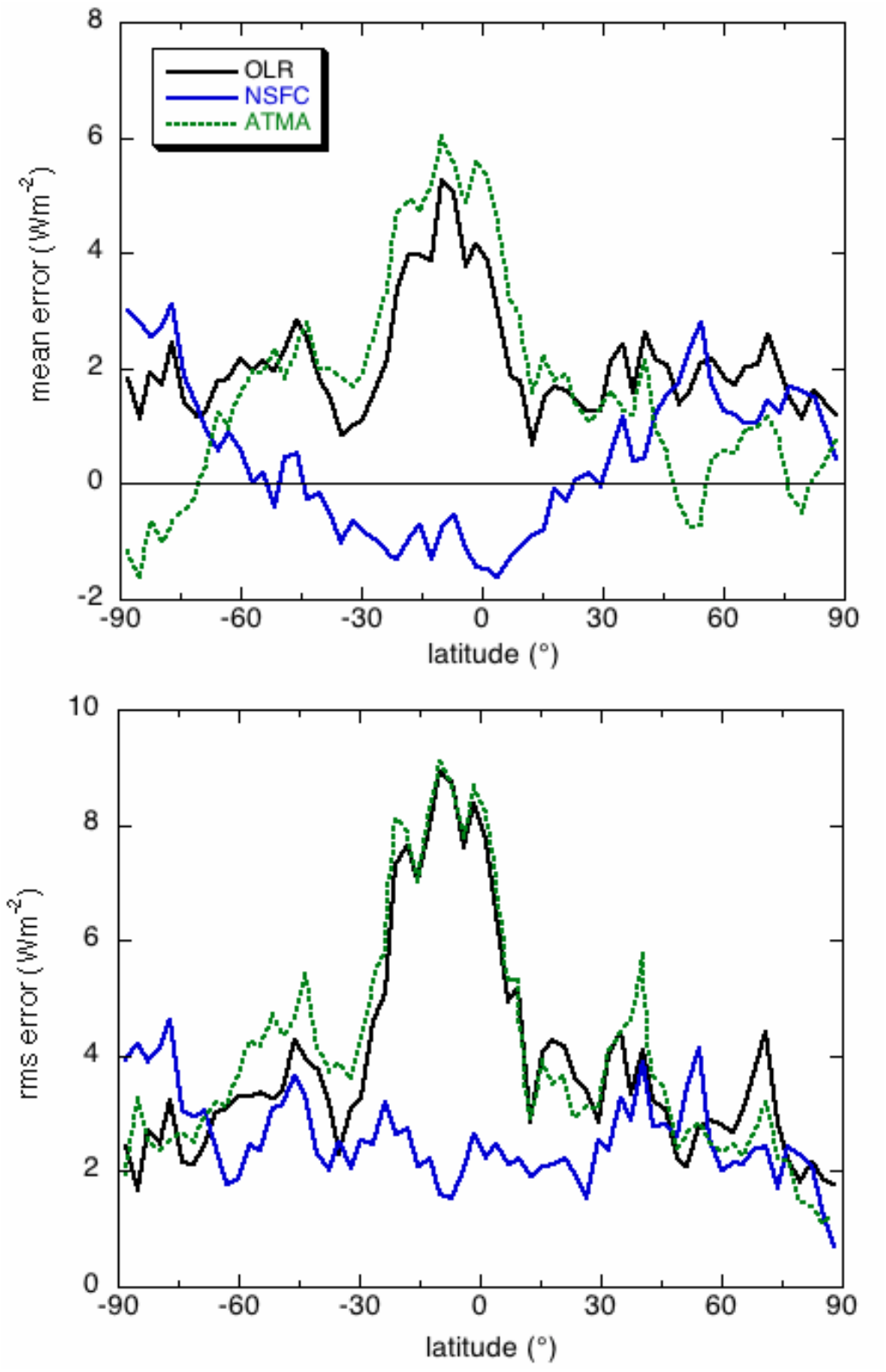

Figure 7. Zonally-averaged LW flux errors of PPH.

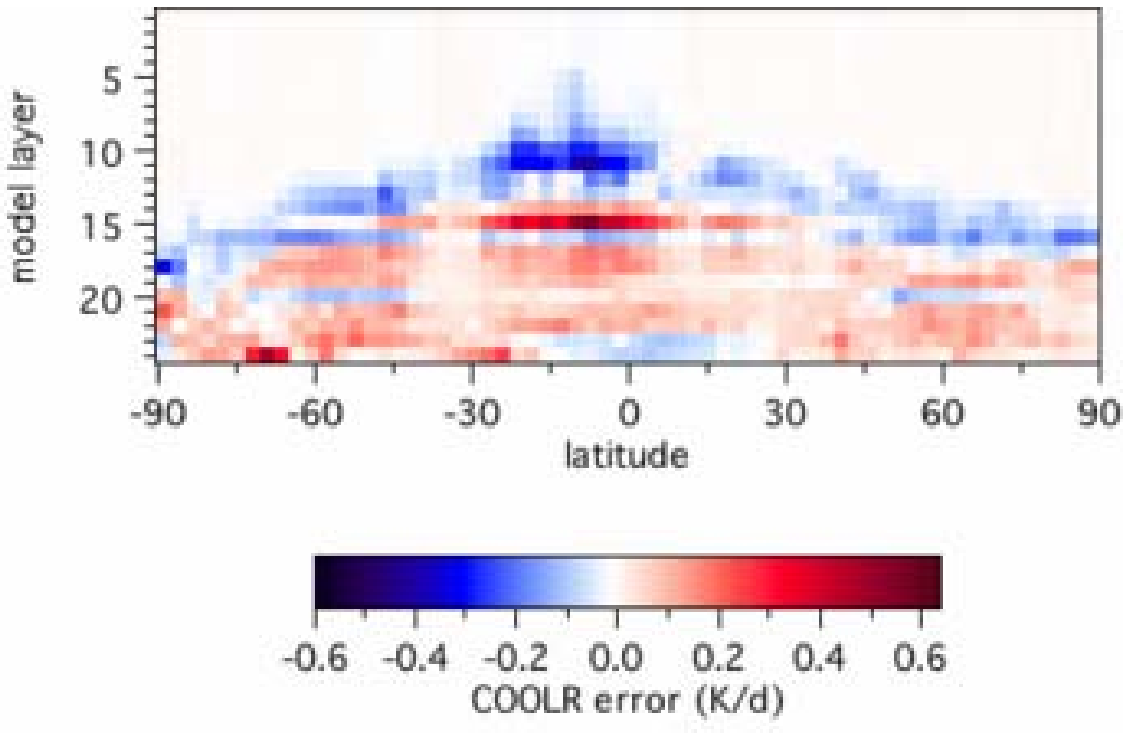

Figure 8. Zonally-averaged LW cooling rate errors of PPH.

References

Barker, H. W., 1996: A parameterization for computing grid-averaged solar fluxes for inhomogeneous marine boundary layer clouds. Part I: Methodology and homogeneous biases. *J. Atmos. Sci.*, **53**, 2289-2303.

Barker, H. W., G. L. Stephens, and Q. Fu, 1999: The sensitivity of domain-averaged solar fluxes to assumptions about cloud geometry. *Quart. J. Roy. Meteor. Soc.*, **125**, 2127-2152.

Cahalan, R. F., W. Ridgway, W. J. Wiscombe, T. L. Bell, and J. B. Snider, 1994: The albedo of fractal stratocumulus clouds. *J. Atmos. Sci.*, **51**, 2434 -2455.

Chou, M.-D., M. J. Suarez, C.-H. Ho, M. M.-H. Yan, and K.-T. Lee, 1998: Parameterizations for cloud overlapping and shortwave single-scattering properties for use in general circulation and cloud ensemble models. *J. Climate*, **11,** 202-214.

Chou, M.-D., and M. J. Suarez, 1999: A shortwave radiation parameterization for atmospheric studies. *NASA Tech. Memo.*, **15**(104606), p. 42.

Chou, M.-D., M. J. Suarez, X.-Z. Liang, and M. M.-H. Yan, 2001: A thermal infrared radiation parameterization for atmospheric studies. *NASA Tech. Memo.*, **19**(104606), p. 55.

Chou, M.-D., K.-T. Lee, and P. Yang, 2002: Parameterization of shortwave cloud optical properties for a mixture of ice particle habits for use in atmospheric models. *J. Geophys. Res.*, **107(D21)**, 4600, doi:10.1029/2002JD002061, AAC 22-1- AAC 22-9.

Harshvardhan, D. A. Randall, and T. G. Corsetti, 1987: A fast radiation parameterization for atmospheric circulation models. *J. Geophys. Res*., **92**, 1009-1016.

Khairoutdinov, M. F., and D. A. Randall, 2001: A Cloud Resolving Model as a cloud parameterization in the NCAR Community Climate System Model: Preliminary results. *Geophys. Res. Lett*., **28**, 3617-3620.

Khairoutdinov, M. F., and D. A. Randall, 2003: Cloud resolving modeling of the ARM Summer 1997 IOP: Model formulation, results, uncertainties, and sensitivities. *J. Atmos. Sci.*, **60**, 607-625.

Khairoutdinov, M. F., D. A. Randall, and C. DeMott, 2003: Simulations of the atmospheric general circulation using a Cloud-Resolving Model and a super-parameterization of physical processes. *J. Atmos. Sci.*, submitted.

Li, J., and H. W. Barker, 2002: Accounting for unresolved clouds in a 1D infrared radiative transfer model. Part II: Horizontal variability of cloud water path. *J. Atmos. Sci.*, **59**, 3321–3339.

McFarquhar, G. M., 2001: Comments on "Parametrization of effective sizes of cirrus-cloud particles and its verification against observations," by Z. Sun, and L. Rikus. *Quart. J. Roy. Meteor. Soc.*, **127**, 261-266.

Oreopoulos, L., and H. W. Barker, 1999: Accounting for subgrid-scale cloud variability in a multi-layer 1D solar radiative transfer algorithm. *Quart. J. Roy. Meteor. Soc.*, **126**, 301-330.

Räisänen, P., 1999: Effect of vertical resolution on cloudy-sky radiation calculations: Tests with two schemes. *J. Geophys. Res.*, **104**, 27,407-27,419.

Szczodrak, M., P. H. Austin, and P. B. Krummel, 2001: Variability of optical depth and effective radius in marine stratocumulus clouds**.** *J. Atmos. Sci.*, **58**, 2912–2926.